Gd(DOTA)-grafted submicronic polysaccharide-based particles functionalized with fucoidan as potential MR contrast agent able to target human activated platelets.

Laura Marcela Forero Ramirez, Elise Gobin, Rachida Aid-Launais, Clément Journe, Fernanda Moraes, Luc Picton, Didier Le Cerf, Didier Letourneur, Cédric Chauvierre, Frédéric Chaubet

Gd(DOTA)-grafted submicronic polysaccharide-based particles functionalized with fucoidan as potential MR contrast agent able to target human activated platelets

Laura Marcela FORERO RAMIREZ[a,b], Elise GOBIN[a], Rachida AID-LAUNAIS[a,c], Clément JOURNE[a,c], Fernanda C. MORAES[a], Luc PICTON[b], Didier LE CERF[b], Didier LETOURNEUR[a], Cédric CHAUVIERRE[a], Frederic CHAUBET[a]±

[a] Laboratory for Vascular Translational Science, UMRS1148, INSERM, Université de Paris, F-75018 Paris, France, Université Sorbonne Paris Nord, F-93430 Villetaneuse, France

[b] Laboratoire Polymères Biopolymères Surfaces, CNRS UMR 6270 & FR3038, Normandie Université, Université de Rouen, INSA de Rouen, F-76821 Mont Saint Aignan, France

[c] UMS34 FRIM, X. Bichat Medical School, Université de Paris, F-75018 Paris, France

± Correspondence to: Frederic Chaubet (e-mail: frederic.chaubet@univ-paris13.fr)

Fax : (33) (0) 1-49-40-30-83 Tel : (33) (0) 1-49-40-40-90

Additional Supporting Information will be found in the online version of this article.

ABSTRACT

Early detection of thrombotic events remains a big medical challenge. Dextran-based submicronic particles bearing Gd(DOTA) groups and functionalized with fucoidan have been produced via a simple and green water-in-oil emulsification/co-crosslinking process. Their capacity to bind to human activated platelets was evidenced *in vitro* as well as their cytocompatibility with human endothelial cells. The presence of Gd(DOTA) moieties was confirmed by elemental analysis and total reflection X-ray fluorescence (TRXF) spectrometry. Detailed characterization of particles was performed in terms of size distribution, morphology, and relaxation rates. In particular, longitudinal and transversal proton relaxivities were respectively 1.7 and 5.0 times higher than those of DOTAREM. This study highlights their potential as an MRI diagnostic platform for atherothrombosis.

KEYWORDS

Dextran, fucoidan, MRI, human platelets, crosslinking, submicronic particles.

HIGHLIGHTS

- Polysaccharide matrix contained both fucoidan and dextran gadolinium macrocomplex.
- A simple and green water-in-oil emulsification/crosslinking method was developed.
- Particles are cytocompatible with human endothelial cells.
- Particles successfully targeted activated human platelets via fucoidan/P-selectin interactions.
- Dual T_1/T_2 relaxation properties were confirmed on MRI phantoms.

Author statement

L. M. FORERO-RAMIREZ : conceptualization, investigation, methodology, formal analysis, writing - original draft ; **E. GOBIN** : investigation ; **R. AID-LAUNAIS** : investigation, methodology; **C. JOURNE** : investigation, methodology ; **F. C. MORAES** : investigation, methodology ; **L. PICTON** : conceptualization, validation, writing - review & editing; **D. LE CERF** : conceptualization, validation, resources ; **D. LETOURNEUR** : conceptualization, validation, funding acquisition; **C. CHAUVIERRE** : conceptualization, validation, resources, writing - review & editing ; **F. CHAUBET** : conceptualization, project administration, funding acquisition, supervision, writing - review & editing

1. Introduction

Atherothrombosis remains the leading cause of morbidity and mortality worldwide and represents a major economic burden on health care systems (Herrington et al., 2016; Lozano et al., 2012). Its underlying cause is atherosclerosis, a chronic inflammatory disease characterized by the formation of lipid-rich plaques in the intima of medium and large arteries. While stable plaques remain asymptomatic and relatively harmless, vulnerable plaques may rupture and thrombose causing myocardial infarction, stroke, or sudden death (Schroeder & Falk, 1995; Waxman et al., 2006). There is thus a medical need for non-invasive tests allowing to early detect high-risk plaques and thrombus formation in order to prevent major cardiovascular events.

Magnetic resonance imaging (MRI) has been successfully used to characterize plaque composition, detect arterial thrombi and monitor plaque progression and regression in several animal models of atherosclerosis and in humans (Corti & Fuster, 2011; Leiner et al., 2005; Raggi et al., 2016; Sannino et al., 2014). In routine practice, MRI often requires the use of Gadolinium-based (Gd) contrast agents to enhance relaxation rates of water molecules, which results in better contrast between different biological tissues (Caravan et al., 1999; Yon et al., 2019; Zhou & Lu, 2013). Nevertheless, these contrast agents have major limitations including a short circulation time, a low diffusion and affinity with the interstitial space and a lack of tissue specificity. Important doses are thus necessary to improve imaging contrast, exposing patients to potential side effects (Kuo et al., 2007; Rogosnitzky & Branch, 2016). These limitations can be addressed by combining nanotechnology and molecular imaging strategies. Nanosystems having paramagnetic properties and bearing targeting molecules able to bind specifically to thrombus have gained increased attention as potential imaging probes. Ultra-small particles of iron oxide, micelles, liposomes, and perfluorocarbon nanoparticles have been designed for MRI visualization of several inflammation-related targets, such as macrophages, oxidized low density lipoproteins, endothelial cell expression, plaque neovasculature, apoptosis, and activated platelets

(Amirbekian et al., 2007; Barkhausen et al., 2003; Briley-Saebo et al., 2008; Cai et al., 2010; Li et al., 2010; McAteer et al., 2010; Suzuki et al., 2015; te Boekhorst et al., 2012; van Tilborg et al., 2010).

P-selectin (140 kDa membrane glycoprotein) is an adhesion molecule overexpressed on the surface of activated platelets and inflamed endothelium of atherothrombotic lesions (Bachelet et al., 2009; Sabourel et al., 2014). P-selectin allows the recruitment of leucocytes through the interaction with its main ligand, PSGL-1 (McEver, 2001). Interestingly, fucoidan is a natural sulfated polysaccharide obtained from brown seaweed extract, which has shown a strong and specific affinity for P-selectin (Bachelet et al., 2009; Chollet et al., 2016; Sabourel et al., 2014). In this context, P-selectin and fucoidan appear as an appropriate target-ligand system for the diagnosis of atherothrombosis. One can therefore hypothesize that the assembly of several molecules of fucoidan with particles containing Gd material will result in MRI contrast probes with increased binding on activated platelets. The aim of the present study was to develop novel and biospecific polysaccharide-based submicronic particles (SPs) functionalized with fucoidan and able to bind to human activated platelets for atherothrombosis imaging by MRI (Scheme 1). Dextran, another polysaccharide widely used in the biomedical field (Abir et al., 2004; Lino Ferreira, 2014; Naessens et al., 2005), was chosen as polymer carrier for Gd(DOTA) groups as the contrast moieties. The polysaccharide nature of the designed objects was expected to ensure their haemocompatibility and low toxicity. Among all the works dealing with micro/nanoparticles exclusively composed of polysaccharides, very few examples were designed for MRI and almost all of them were developed for cancer diagnostics. Chitosan and hyaluronic acid have been by far the most employed polysaccharides to get Gd-loaded nanoparticles (Chan et al., 2015; Gheran et al., 2018; Huang et al., 2008; Na et al., 2016; Nam et al., 2010; Payne et al., 2017; Rigaux et al., 2017; Zhang et al., 2015), but alginate and pullulan-based ones have also been described (Kim et al., 2015; Podgórna et al., 2017). They were mainly prepared by self-assembly of amphiphilic polysaccharide derivatives, formation of polyelectrolyte complexes or ionic gelation with sodium tripolyphosphate. To the best of our knowledge,

no polysaccharide-based submicronic particle combining fucoidan and Gd-based contrast agent has been developed yet, which contributes to the originality of the present work.

As a first step, a chemical modification of native dextran to introduce Gd(DOTA) groups was performed. Next, SPs were synthesized by co-crosslinking of fucoidan and former dextran macrocomplexes within the droplets of a water-in-oil emulsion. SPs were characterized in terms of morphology, size and zeta potential. *In vitro* assays were performed to evaluate the cytotoxicity, contrast properties and targeting capacity of the obtained objects.

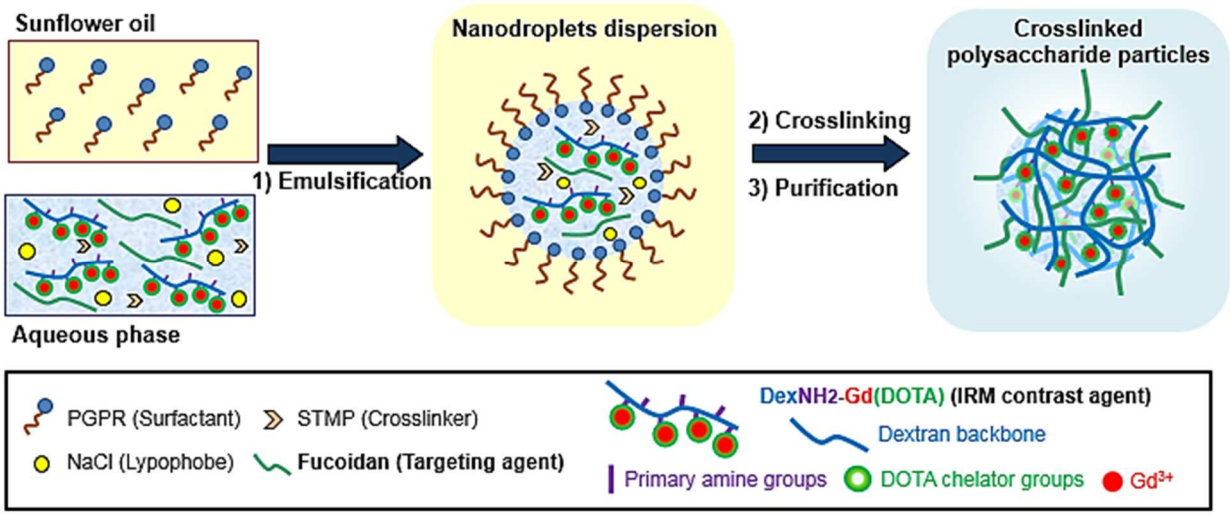

Scheme 1. Preparation of polysaccharide submicron particles via a combined inverse emulsion-crosslinking method.

2. Materials and methods

2.1 Materials

Dextran T70 ($\bar{M}_n$= 55 000 g/mol, Đ = 1.12) was purchased from Pharmacosmos (Holbæk, Denmark), Low molecular weight fucoidan ($\bar{M}_n$ = 4 400 g/mol, Đ = 1.49, 16.8 wt% sulfates) was obtained from

Algues & Mer (Ouessant, France) in the framework of a partnership for the pharmaceutical development of a GMP-grade fucoidan for molecular diagnosis of cardiovascular diseases (Chauvierre et al., 2019). 3-chloropropylamine hydrochloride, 1-ethyl-3-(3-dimethylaminopropyl) carbodiimide hydrochloride (EDC.HCl), N-hydroxysuccinimide (NHS), Gadolinium(III) chloride hexahydrate ($GdCl_3.6H_2O$) and Paraformaldehyde (PFA) were purchased from Fisher Scientific (Illkirch, France). 1,4,7,10-Tetraazacyclododecane-1,4,7,10-tetraacetic acid (DOTA) was provided by Leap Labchem (Hangzhou, China). Ethylenediaminetetraacetic acid (EDTA), Trisodium Trimetaphosphate (STMP), Sodium Dodecyl Sulfate (SDS), Triton X-100, 7-hydroxy-10-oxidophenoxazin-10-ium-3-one (resazurin), 3,3′-Dihexyloxacarbocyanine iodide ($DiOC_6$), 4',6-diamidino-2-phenylindole (DAPI) and Phalloidin-TRITC were from Sigma Aldrich (Saint-Quentin-Fallavier, France). Dextran-FITC ($\bar{M}_w$ = 70 000 g/mol) and Dextran-TRITC ($\bar{M}_w$ = 40 000 g/mol) were from TdB Consultancy (Uppsala, Sweden). Polyglycerol polyricinoleate (PGPR 4150) was a gift from Palsgaard SAS (Lyon, France). Sunflower oil (Lesieur, France) is a mixture of saturated fatty acids (palmitic acid ~5 wt%- and stearic acid ~6 wt%) and unsaturated fatty acids (mainly oleic acid ~37 wt% and linoleic acid ~51 wt%). Thrombin receptor-activating-peptide (TRAP) was obtained from PolyPeptide laboratories (Strasbourg, France). PE-CyTM5 mouse anti-human CD41a was provided by BD Pharmingen, (Le Pont de-Claix, France), mouse anti-human CD62P and mouse anti-human CD62P-FITC were obtained from Beckman Coulter (Villepinte, France). Tyrode-Hepes buffer (0.3 wt% BSA, pH 7,24) contained 137 mM NaCl, 2 mM KCl, 12 mM $NaHCO_3$, 0.3 mM Na_2HPO_4, 5.5 mM glucose and 5 mM Hepes. All materials were used without further purification. Dialysis membranes of 10 000 Da were purchased from Spectrum Laboratories (New Brunswick, NJ, USA).

2.2 Preparation of DexNH_2-Gd(DOTA) complexes

Dextran derivatives bearing Gd(DOTA) groups were synthesized in three steps (Scheme 2). In the first step, the attachment of primary amine functions (NH_2) onto dextran was performed in aqueous basic

media. Typically, 5 g of dextran (31 mmol of anhydroglucopyranose unit (AGU)) were dissolved in 25 mL of water. 25 mL of NaOH (6.2M) were added and the mixture was stirred during 30 minutes. The reaction flask was then immersed in a thermostated oil bath at 55 °C before the addition of 8 g of 3-chloropropylamine hydrochloride (62 mmol, 2 equivalents per AGU) and the mixture was maintained under stirring during different reaction times. After neutralization, the polymer ($DexNH_2$), was extensively dialyzed against ultrapure water (cut-off: 10 000 Da) and finally freeze-dried. Degree of substitution of primary amine groups per 100 AGU (DS_{NH2}) was estimated by elemental analysis of nitrogen.

In the second step, DOTA groups were linked to aminated dextran using classical EDC/NHS reaction. Typically, DOTA (1 equivalent per primary amine group) was dissolved in 10 mL of water and pH was adjusted to 3.5 with diluted HCl (0.5M). After 30 min of stirring, EDC and NHS were added at a molar ratio DOTA/EDC/NHS of 1/5/1.25. The pH was raised to 7 and $DexNH_2$ previously dissolved in 10 mL of water was added in small amounts for 1h. The mixture was stirred at room temperature for 2h. Resulting $DexNH_2$-DOTA derivative was dialyzed against EDTA (0.05M) to avoid the complexation of contaminating metal ions by DOTA then against water (cut-off: 10 000 Da) before freeze-drying. Degree of substitution of DOTA moieties per 100 AGU (DS_{DOTA}) was estimated from the increase of nitrogen content with respect to the one of $DexNH_2$ precursor.

In the third step, the chelation of Gd^{3+} ions by DOTA groups along the dextran backbone was performed by mixing $GdCl_3.6H_2O$ (1 Gd^{3+} per DOTA group) with $DexNH_2$-DOTA in water as previously described (Nguyen et al., 2017). After adjusting the pH to 6.5 with NaOH, the solution was maintained at room temperature overnight followed by heating at 60 °C for 4h. Chlorides were removed by dialysis (cut-off: 10 000 Da) and white fluffy products were obtained after freeze-drying. Dextran gadolinium chelates were called $DexNH_2$-Gd(DOTA). Degree of substitution of Gd^{3+} ions per 100 AGU (DS_{Gd}) was determined by total reflection X-ray fluorescence (TRXF) spectrometry (S2 Picofox, Bruker, Germany).

170 *2.3 Polysaccharide submicron particles synthesis*

171 Dextran T70 particles were obtained via a water-in-oil emulsification-crosslinking method inspired from
172 our previous works (Bonnard et al., 2014). Typical experimental conditions were as follows: 1.2 g of
173 dextran and 1.4 g of NaCl were solubilized in 4 mL of water. 1.2 g of this solution were then mixed with
174 120 µL of NaOH (10M) and 240 µL of trisodium trimetaphosphate (STMP) (30% (w/v) in water). 300 µL
175 of the mixture were slowly injected into 15 ml of sunflower oil containing 6.0% (w/v) of polyglycerol
176 polyricinoleate (PGPR) as emulsion stabilizer and dispersed with a homogenizer at 30,000 rpm for 4 min
177 (Polytron PT 3100, dispersing aggregate PT-DA 07/2EC-B101, Kinematica, Luzernerstrasse,
178 Switzerland). The resulting emulsion was then transferred to an oven (50 °C) wherein the crosslinking
179 step took place for 20 min. Polysaccharide particles were recovered by ultracentrifugation (15,000 g, 45
180 min), washed once with PBS 1X, twice with SDS (0.04% (w/v)) and four times with water. The resulting
181 pellets were resuspended in water and stored at 4 °C until use. To prepare Gd-loaded particles (Gd-SPs),
182 dextran was replaced by $DexNH_2$-Gd(DOTA). Fucoidan-functionalized particles (FUCO-Gd-SPs) were
183 prepared with 60 mg of fucoidan and 1.14 g of $DexNH_2$-Gd(DOTA).

184 *2.4 Physico-chemical characterizations*

185 ^1H NMR spectra were recorded on a Bruker-400 Ultrashield (Bruker, Germany). Samples were prepared in
186 D_2O at a concentration of 20 mg/mL.

187 Average molecular weight of dextran derivatives was determined by size exclusion chromatography
188 coupled to a multi-angle laser light scattering detector (SEC-MALLS) in $NaNO_3/NaN_3$ (0.15 M/0.02%
189 (w/v)). Refractive index increment (dn/dc) of 0.146 $mL.g^{-1}$ was used (See Supporting).

190 The viscosities of sunflower oil and dextran solutions were measured at 25 °C using a rotational
191 rheometer with a concentric cylinder geometry (TA instrument HR2, Delaware, USA).

Nitrogen content was estimated by elemental analysis (Service de Microanalyse du CNRS, ICSN, Gif-sur-Yvette, France). Phosphorus and gadolinium contents were determined by total reflection X-ray fluorescence (TRXF) spectrometry (S2 PICOFOX, Bruker, Germany). Fucoidan content was assessed by colorimetric quantification of sulfates as previously described (Li et al., 2017).

Particle size distribution was measured by using Laser Diffraction Particle Size Analyzer (Mastersizer 3000, Malvern Instruments, UK) and number distributions are reported. The obtained size (D50) and span values were an average of at least three consecutive measurements.

Zeta potential of particles was measured in 1mM KCl at 25°C using a Zetasizer Nano-ZS (Malvern Instruments, Malvern, UK).

The morphology of particles was investigated by Transmission Electron Microscopy (TEM, Tecnai 12, 80 kV; FEI; Hillsboro, OR, USA), Scanning Electron Microscopy (SEM, Philips XL30 ESEM-FEG, Netherlands) and confocal microscopy (Zeiss LSM 780 with 63× oil objective, Carl Zeiss Microscopy, Oberkochen, Germany). For TEM observation, 3 µL of particles suspension were dropped onto a 400 mesh copper grid and positive stained with uranyl acetate (1% (w/v)) and allowed to air-dry at room temperature. For SEM images, one drop of particles suspension was dropped onto a silicon wafer, then air-dried and coated with a thin layer of gold before observation.

2.5 Cytotoxicity tests

Human Umbilical Vein Endothelial Cells (HUVECs) were grown in DMEM supplemented with 10% (v/v) fetal bovine serum, 4mM of L-glutamine, 100 U/mL penicillin and 100 µg/mL streptomycin. Cells were cultivated at 37 °C under 5% CO_2 (v/v) in a humidified incubator. HUVECs were seeded at 10,000 cells per well in 96-well plates and incubated for 24h. After that, culture medium was removed and 100 µL of particle suspensions at different concentrations (200, 500 and 1 000 µg/mL) were added. Cells metabolic activity was determined after 24h by resazurin assay. Cells were incubated with medium

containing 10% resazurin for 2h at 37 °C and fluorescence intensity (λex = 560 nm; λem = 590 nm) was read in an Infinite M200 PRO microplate (TECAN Group Ltd, Switzerland). Metabolic activity in the presence of particles was compared to the control condition.

To assess cells morphology, samples were fixed with PFA and incubated with TRITC-phalloidin and DAPI to stain for F-actin and nuclei respectively.

2.6 MRI phantoms

DOTAREM, DexNH_2-Gd(DOTA) and FUCO-Gd-SPs gel phantoms (Gd concentrations ranging between 0.12 and 1.0 mM) were prepared in 0.5 mL tubes using 2% (w/v) agarose. These tubes were put inside of a larger container, which was itself filled with agarose gel.

Longitudinal relaxation (T_1) and transversal relaxation (T_2) times were acquired on a 7 Tesla animal MR imager (Pharmascan 70/16, Bruker Biospin, Ettlingen, Germany), and analyzed with Bruker software Paravision 6.0.1. In order to calculate T_1 map, a rapid acquisition with relaxation enhancement (RARE) sequence was used, with echo time (TE) of 8.5 ms, variable repetition time (TR, 200, 400, 800, 1500, 3000, 5500 ms), matrix (MTX): 128x128, field of view (FOV): 30x30 mm and slice thickness of 1 mm. For T_2 map calculation, a multislice multiecho (MSME) sequence was employed with TR of 2200 ms and TE between 6.8 to 170 ms (25 echoes; echo spacing: 6.8 ms). MTX, FOV and slice thickness were as before. The slope of the line obtained by plotting the relaxation rates R1 and R2 (R1= 1/T1; R2 = 1/T2) at different concentration, provided the relaxivity r_1 and r_2 respectively.

2.7 Interaction of SPs with human activated platelets

2.7.1 Under static conditions

The interaction between three groups of PE-Cy5 labeled platelets (non-activated platelets (PRP), activated platelets (PRP + TRAP) and P-selectin blocked activated platelets (PRP + TRAP + anti-CD62P)) and

FUCO-Gd-SPs was measured by flow cytometry. Protocol was adapted from (Li et al., 2017). Briefly, 5 mL of blood from healthy adult volunteers were collected in sodium citrate 3.8% (w/v). Platelet-rich plasma (PRP) was obtained by centrifugation at 200 g for 15 min (5702RH centrifuge Beckman Coulter, Villepinte, France) and platelet concentration was adjusted to 1×10^8 ml^{-1} with Tyrode-HEPES buffer (0.3 wt% BSA). Platelets were labeled by incubation with PE-CyTM5 mouse anti-human CD41a for 15 min. Conjugate excess was then eliminated by a wash step. Activated PRP was obtained by stimulation of PRP with 20 µM TRAP. In some experiments, activated then P-selectin-blocked PRP were obtained by incubation with a non-labeled anti-human CD62P at high concentration (0.04 mg/mL). Before assessing the interaction with particles, P-selectin expression level at the platelet surface was assessed using an anti-human CD62P-FITC and measuring FITC signal by flow cytometry. To evaluate the binding ability of particles to P-selectin expressed onto platelets, 5 µL of nonactivated PRP, activated PRP with TRAP or anti P-selectin-treated activated PRP were incubated for 20 min with 5 µl of FITC-labeled FUCO-Gd-SPs (10 mg/mL). Sample volume was then completed to 100 µL using Tyrode-HEPES buffer (0.3 wt% BSA). Samples were analyzed on a LSRII flow cytometer (BD Biosciences, Le Pont de Claix, France), 10,000 PE-Cy5 positive platelets were collected per sample, and the mean fluorescence intensity (MFI) of FITC channel was measured in these platelets. FITC-labeled Gd-SPs were used as negative control.

2.7.2 Under arterial flow conditions

Binding ability of FUCO-Gd-SPs to P-selectin expressed on activated platelet aggregates was as well evaluated *in vitro* as previously reported (Li et al., 2017; Juenet et al., 2018). Briefly, micro-channels of Vena8 Fluoro+ chambers (Cellix Ltd, Dublin, Ireland) were coated overnight with 50 µg/mL of collagen and then washed with NaCl 0.9%. Human whole blood labeled with $DiOC_6$ (a green fluorescent dye) was perfused under arterial flow conditions for 5 min to induce platelet activation and aggregation on the collagen-coated channel. TRITC labeled FUCO-Gd-SPs at 1 mg/mL in NaCl 0.9% were then perfused during 5 min. Their accumulation onto preformed platelet aggregates was monitored in real time by

fluorescence microscopy (Axio Observer, Carl Zeiss Microscopy, Oberkochen, Germany). Fluorescence images were taken along each micro-channel after washing with NaCl 0.9%. Gd-SPs were used as negative control.

2.8 Statistical Analysis

Data are presented as mean ± SEM (n≥3). Flow cytometry results were analyzed statistically with a one-way ANOVA with Bonferroni post-tests to compare data obtained with Gd-SPs and Fuco-Gd-SPs. A difference of $p < 0.05$ was considered significant.

3. Results

3.1 Synthesis of dextran gadolinium chelates.

A series of aminated dextran ($DexNH_2$), dextran ligands ($DexNH_2$-DOTA) and their corresponding gadolinium complexes ($DexNH_2$-Gd(DOTA)) were synthesized in three consecutive steps (Scheme 2). All modifications were done in aqueous media. Three sets of reaction conditions were used (Conditions-1, 2, 3), resulting in three final macrocomplexes named Complex-1, 2, 3, respectively. The substitution degrees (DS) of primary amines, DOTA groups and Gd^{3+} ions were expressed as the number of introduced groups per 100 AGU. All physicochemical characterizations are reported in Table 1.

Amination of dextran was performed in basic solution (3.1 M NaOH) by reaction with 3-chloropropylamine leading to $DexNH_2$ derivatives (1st step, Table 1). Successful introduction of amine moieties was confirmed by elemental analysis of nitrogen content (%N) and ^{1}H NMR spectroscopy. The characteristic peaks of methylene protons of propylamine group (-CH_2-C**H**$_2$-C**H**$_2$-NH_2) were clearly visible at 1.9 ppm and 3.1 ppm (Figure S1). Substitution degree of amine (DS_{NH2}) could be tuned from 5.6 to 23.9% by increasing reaction time (1.5, 3 and 14 h) at constant amine/AGU feeding ratio (2/1).

These results are in agreement with those reported by De Nooy et al. for the amination of scleroglucan (De Nooy et al., 2000). Furthermore, no degradation of the dextran backbone under basic conditions (pH≈13) was evidenced at early times and only a slight decrease in molecular weight was observed at 14 h as attested by SEC-MALLS analysis (Table S1).

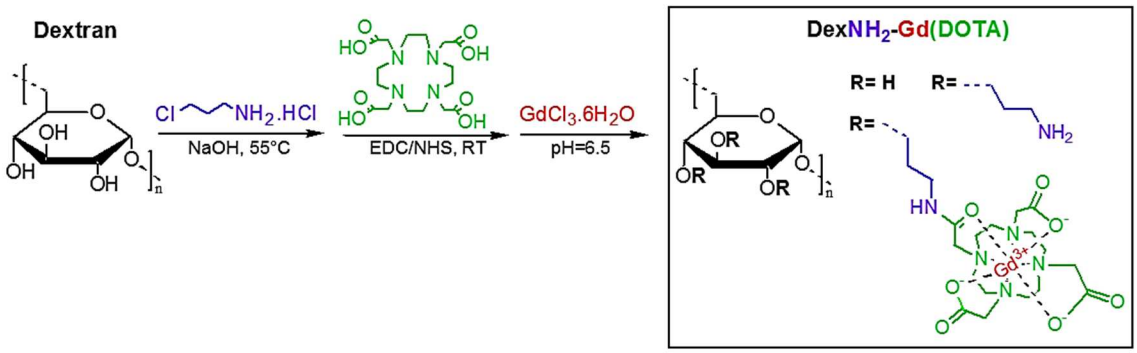

Scheme 2. Synthesis of $DexNH_2$-Gd(DOTA) complexes.

Table 1. Physicochemical characteristics of $DexNH_2$-Gd(DOTA) complexes.

	1st step Amination ($DexNH_2$)			2nd step DOTA attachment ($DexNH_2$-DOTA)			3rd step Gd complexation ($DexNH_2$-Gd(DOTA))		Resultant derivative		
					DS (%)						
Reaction set	t (h)	%N[a] (wt)	DS_{NH2}[b] (%)	%N[a] (wt)	NH_2r[b]	DOTA[b]	%Gd[c] (wt)	DS_{Gd}[d] (%)		$\bar{M}_{n\ exp}$[e] (g/mol)	Đ[e]
Conditions-1	1.5	0.48±0.05	5.6	1.27±0.04	3.0	2.6	2.0±0.1	2.4	Complex-1	67 000	1.5
Conditions-2	3.0	0.65±0.03	7.7	2.12±0.03	2.6	5.1	4.0±0.2	5.0	Complex-2	75 000	1.7
Conditions-3	14	1.90±0.10	23.9	3.54±0.09	17.1	6.8	4.9±0.2	6.7	Complex-3	73 000	1.6

(a) Nitrogen content estimated by elemental analyses. (b) Degree of substitution of initial primary amines (NH_2), residual primary amines (NH_2r, not modified with DOTA groups) and grafted DOTA moieties (DS_{DOTA}) per 100 AGU were calculated from N content (DS_{NH2r} + DS_{DOTA} = DS_{NH2}). (c) Gadolinium content determined by total reflection X-ray fluorescence (TRXF) spectrometry. (d) Degree of substitution of gadolinium ions per 100 glucopyranose units estimated from Gd content. (e) Evaluated from SEC-MALLS in $NaNO_3$/NaN_3 (0.15 M/0.02% (w/v)) with dn/dc=0.146 mL/g.

297 EDC/NHS chemistry was used to graft DOTA ligands to amine functions of $DexNH_2$. Higher
298 nitrogen content of resultant $DexNH_2$-DOTA derivatives (with respect to the corresponding
299 $DexNH_2$ precursors) confirmed the incorporation of the DOTA tetraazamacrocycle (2^{nd} step,
300 Table 1). Initial quantity of amine functions (DS_{NH2}) was shown to influence both the degree
301 of substitution DS_{DOTA} and the grafting yield. As expected, the number of DOTA groups
302 linked to dextran chains increased with the initial amine content, all other conditions being the
303 same. In all cases, DOTA grafting was incomplete leaving unreacted propylamines along
304 dextran backbone. Coupling yields were in about 50-60% for initial DS_{NH2} values below 8%
305 (Conditions-1 and 2, Table 1) and of less than 30% when DS_{NH2} was equal to 23.9%
306 (Conditions-3). This low yield was likely due to steric hindrance effects.

307 $DexNH_2$-Gd(DOTA) macrocomplexes were finally produced by reacting former $DexNH_2$-
308 DOTA ligands with gadolinium chloride (3^{rd} step, Table 1). An aminated dextran (without
309 DOTA groups) was used as negative control. The amount of complexed Gd^{3+} was assessed by
310 TXRF. According to X-ray fluorescence emission spectra, Gd was effectively chelated by
311 $DexNH_2$-DOTA ligands while no Gd was detected in the case of aminated dextran (Figure
312 S2). These results further demonstrated the presence of DOTA moieties covalently linked to
313 the polysaccharide. In addition, DS_{Gd} calculated from Gd content (%Gd) matched well with
314 DS_{DOTA} previously estimated from N content, indicating the presence of one Gd^{3+} ion per
315 DOTA group. Three $DexNH_2$-Gd(DOTA) complexes having 2.4 (Complex-1), 5.0 (Complex-
316 2) and 6.7 (Complex-3) Gd(DOTA) groups per 100 AGU were obtained corresponding to 8,
317 17 and 23 Gd(DOTA) groups per dextran chain, respectively.

3.2 Preparation of polysaccharide-based submicronic particles

3.2.1 Optimization of crosslinking and emulsion conditions

Polysaccharide-based particles were prepared in one-step using a combined water-in-oil emulsion/co-crosslinking process. This process was solvent-free in both production and purification steps. Sunflower oil was used as continuous phase instead of organic solvents commonly reported in the literature. Furthermore, STMP and PGPR, safe materials with no reported adverse effects on humans (Abed et al., 2011; Nikolovski et al., 2016), were used as crosslinking agent and emulsion stabilizer respectively.

Native dextran (Dextran T70) was used as a model polysaccharide to optimize the preparation of particles. Crosslinking reaction was performed at 50°C at constant 1M NaOH concentration. SEC/MALLS measurements indicated that no degradation of dextran backbone occurred during 5h under these conditions (Table S2). The use of sodium chloride (4M) appeared to increase the reaction rate. NaCl screened phosphate negative charges coming from STMP reaction keeping macromolecular chains closer, thus improving the crosslinking process.

We determined the lower polysaccharide and STMP concentrations required to succesfully crosslinked dextran chains. For a dextran solution at about or below 120 g/L no gelation was noted. This result was expected as the critical overlap concentration (C*) of Dextran T70 in water is reported at about 112 g/L at 40°C (Antoniou & Tsianou, 2012). Stable 3D networks were obtained for dextran concentrations equal or above 200 g/L since the entanglement density of dextran chains was sufficient in such conditions. Minimal [STMP]/[AGU] molar ratio required for crosslinking was equal to 0.02. Below this value, no reaction occurred.

340 The viscosity of both dispersed (η_d) and continuous phases (η_c), and more specifically the
341 viscosity ratio (η_d/η_c) play an important role in droplets size, dispersity and stability.
342 Typically, the emulsification process is highly intensified when that ratio tends to 1 and
343 smaller droplets can be obtained (Vananroye et al., 2006). On one hand, regarding continuous
344 phase, sunflower oil viscosity was 16 mPa.s at 25 °C and increased slightly to 19 mPa.s with
345 the addition of 6% (w/v) of PGPR. On the other hand, dextran solutions containing 4M NaCl
346 behaves like Newtonian fluids (i.e. viscosity does not depend on the shear rate) in the
347 concentration range studied (50-500 g/L) (Figure S3a). As the concentration of solutions
348 increased from 50 to 500 g/L, the relative viscosity increased exponentially from 1.6 to 163
349 (Figure S3b). An aqueous phase containing 200 g/L of dextran, giving a viscosity of 12 mPa.s
350 and a viscosity ratio η_d/η_c of ~0.6, was finally chosen for the preparation of particles.

351 *3.2.2 Tuning particles size*

352 Table 2 summarizes experimental conditions used in the present study (Runs 1-5), as well as
353 the average size of the particles after purification and resuspension in water. In all
354 formulations, aqueous phase contained 200 g/L of polysaccharide and 1M NaOH while
355 continuous phase was composed of sunflower oil and PGPR (6% (w/v)). Water to oil phases
356 ratio was kept to 30/150 (v/v). Phosphorus content (%P) in as-obtained particles was used as
357 indicator of the actual amount of phosphoester groups incorporated in the polymer network
358 (i.e. intermolecular, intramolecular and monografted) (Lack et al., 2007; Dulong et al., 2011).

359 Particles size was tuned by varying STMP concentration and consequently [STMP]/[AGU]
360 molar ratio (Runs 1-3). Unsurprisingly, the higher the initial [STMP]/[AGU] ratio, the smaller
361 the particle size. This observation can be correlated to the increase of crosslinking as
362 suggested by the rise of P content. More densely packed particles with lesser swelling in
363 water were obtained at higher STMP feeding amount. Because of the anionic charges brought

by STMP, all particles exhibited negative zeta potential. Submicronic particles (SPs) of about 790 nm with narrow size distribution can be achieved in a reproducible way by using [STMP]/[AGU]=0.17 (6.0 % (w/v) STMP, Run 3). Production yield was of about 35%.

Table 2. Formulation and physico-chemical characterization of polysaccharide submicronic particles. Crosslinking reaction was performed at 50°C during 20 min with [Polysaccharide]=200 g/L [NaOH]=1M, [PGPR]= 6% (w/v).

R.	Polysaccharide	$\frac{[STMP]}{[AGU]}$	D(nm)	Span [(a)]	Zeta potential (mV)	%P [(b)]	%Gd [(b)]
1	$DexT_{70}$	0.043	1720±50	0.61±0.01	-18±3	0.6±0.1	-
2	$DexT_{70}$	0.087	1230±45	0.67±0.03	-22±3	0.8±0.1	-
3	$DexT_{70}$	0.170	790±30	0.61±0.01	-30±3	1.1±0.1	-
4	Complex-2	0.170	720±35	0.67±0.03	-28±5	1.0±0.1	2.6±0.2
5	Complex-2/Fuco	0.170	840±45	0.60±0.02	-25±4	1.1±0.1	2.3±0.1

(a) Width of the distribution calculated using $Span = (D(0.9) - D(0.1))/ D(0.5)$. D(0.1), D(0.5) and D(0.9) were the particle diameters at 10%, 50% and 90% of the particle number size distribution. (b)Determined by Total Reflection X-ray Fluorescence (TXRF).

3.2.3 Synthesis of Gd-SPs and FUCO-Gd-SPs

The optimized emulsion conditions described above (Run 3) were applied to gadolinium Complex-2 (Table 1) to obtain two types of SPs: non-functionalized/Gd-loaded SPs (Gd-SPs, Run 4) and fucoidan-functionalized/Gd-loaded SPs (FUCO-Gd-SPs, Run 5). For dextran derivatives with higher modification degrees (Complex-3), no gel was obtained. This was likely due to a reduced amount of hydroxyl groups available for crosslinking and to steric hindrance. Complex-2 was chosen over Complex-1 because of its higher Gd content.

Size distribution, zeta potential and %P of Gd-SPs and FUCO-Gd-SPs were roughly like those obtained with model SPs (Run 3). Gd content was similar for both types of SPs (2.3-2.6 wt%) but almost 2-times lower than the one of dextran complex precursor (4.0 wt%). Alkaline

crosslinking conditions would led to some hydrolysis of amide bonds linking Gd(DOTA) groups to dextran and to a loss of Gd(DOTA) moieties. This hypothesis was supported by the decrease in nitrogen content (around 1.70 wt% in SPs compared to 2.12 wt% in Complex-2). FUCO-Gd-SPs contained 23±5 µmol S/g which corresponded to a fucoidan content of 1.3 wt% (about 26 wt% of the fucoidan initially dissolved in the aqueous phase).

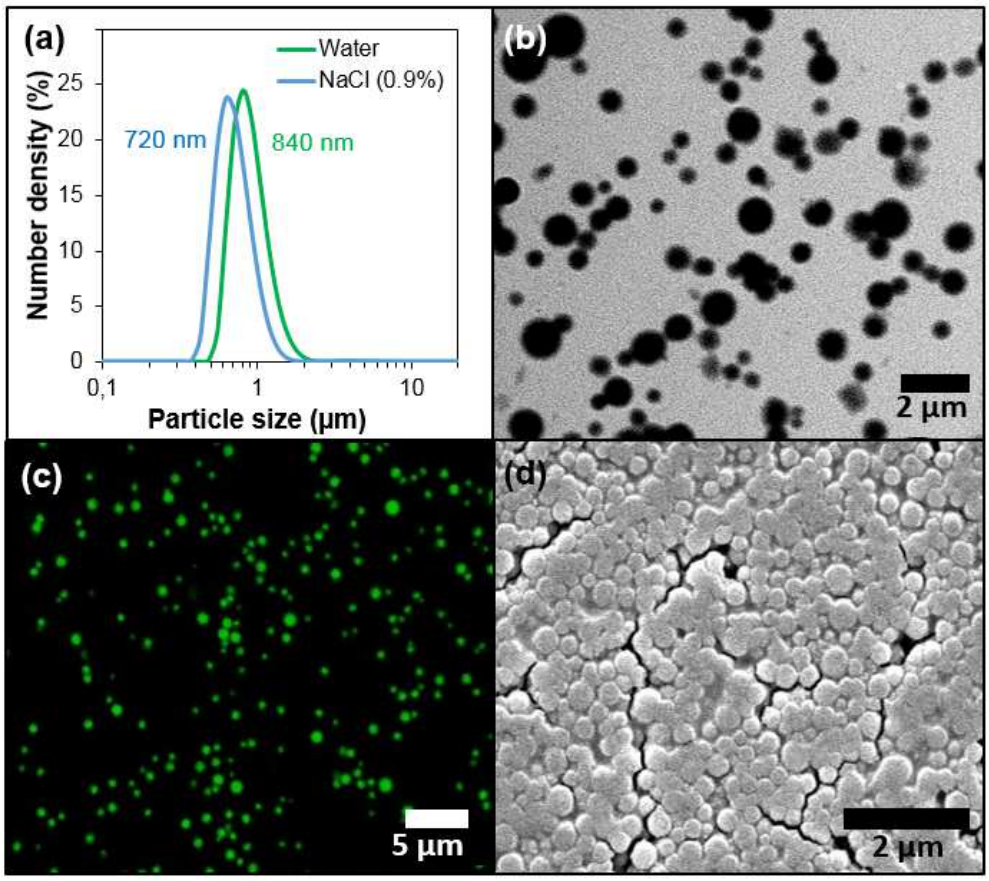

Figure 1. a) Size distribution in water and NaCl 0.9% and b) TEM c) Confocal microscopy and d) SEM-Micrographs of FUCO-Gd-SPs. In the case of confocal microscopy, sample was analyzed in its hydrated state. For the other techniques (TEM and SEM), SPs were air-dried and submitted to vacuum conditions.

TEM, SEM and confocal micrographs of FUCO-Gd-SPs are depicted in Figure 1b-d. All techniques confirmed the production of spherical and homogeneous objects in the

submicronic range. Average particles sizes observed by confocal microscopy agreed with those measured by laser diffraction (~800 nm) whereas smaller average sizes were detected by TEM (~700 nm) and SEM (~400 nm). These differences arise from sample preparation (in hydrated or dried states) and observation conditions (vacuum).

The FUCO-Gd-SPs were stable for at least two weeks when stored in aqueous suspension at 4 °C. In addition, the effective protection of particle size during freeze-drying can be ensured with 5% (w/v) sucrose as cryoprotectant since no aggregation was observed after resuspension in aqueous medium. This allowed long-term storage of SPs. As expected, FUCO-Gd-SPs average size was found to be smaller in physiological saline solution (0.9% NaCl) because of the screening of phosphate negative charges (Figure 1a). The FUCO-Gd-SPs remained stable at room temperature and 37 °C for at least 72h under such conditions.

3.3 Cytotoxicity

Cytocompatibility of Complex-2 (Table 1) toward HUVECs was checked and compared with the one of free Gd^{3+} ions (concentration ranging from 8 to 80 µg/mL). Cell viability was assessed by measuring metabolic activity of the mitochondria using resazurin reagent. Complex-2 did not affect cell viability after 24h. In contrast, metabolic activity decreased down to 50% in the presence of free Gd^{3+} (Figure S4). Mitochondrial dysfunction induced by Gd^{3+} and other lanthanide ions has been already reported (Feng et al., 2010; Liu et al., 2003; Zhao et al., 2014). These results further proved the successful chelation of Gd^{3+} by DOTA groups of $DexNH_2$-DOTA derivatives.

FUCO-Gd-SPs also showed excellent cytocompatibility even at concentrations at high as 1 mg/mL (Figure 2a). No major morphological changes of HUVECs were evidenced when compared to control conditions (Figure 2b). Furthermore, FUCO-Gd-SPs appeared to be

internalized by endocytosis. Particles engulfment by HUVECs was clearly seen by confocal microscopy (Figure 2c). Further *in vitro* and *in vivo* studies will be required for a complete understanding of the mechanism involved in internalization, as well as the fate of the particles.

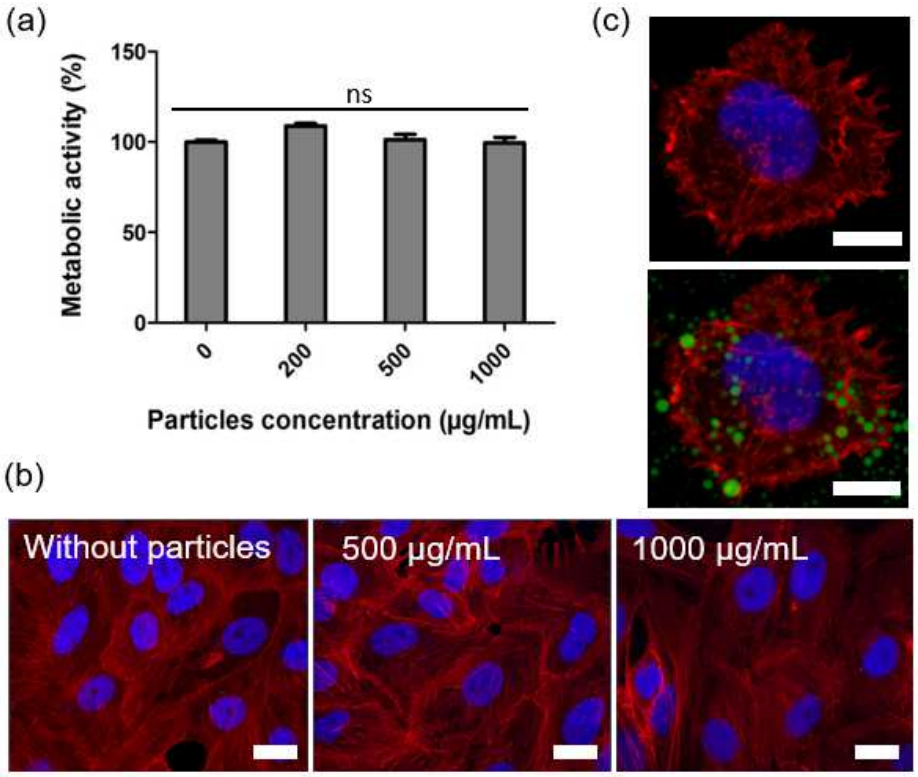

Figure 2. a) Cytocompatibility of FUCO-Gd-SPs towards HUVECs after 24 h incubation at 37°C. 100% of mitochondrial metabolic activity (resazurin reduction assay) corresponds to control cells incubated without particles. n = 3. b) Fluorescent images of HUVECs. F-actin is shown in *red* (TRITC-Phalloidin) and nuclei are shown in *blue* (DAPI), white scale bar corresponds to 20µm c) Zoom on an isolated cell evidences the internalization of the fluorescent particles. White scale bar corresponds to 10µm.

3.4 Proton relaxation effects of dextran derivatives and FUCO-Gd-SPs

The efficiency of an MRI contrast agent is correlated to its relaxivity. That is, its ability to accelerate longitudinal ($1/T_1$) or transversal ($1/T_2$) relaxation rates of the protons of hydrogen atoms from the surrounding water molecules (Jacques et al., 2010). Relaxometric properties of Complex-2 and FUCO-Gd-SPs were assessed *in vitro* on agarose phantoms at 7 Tesla. Commercially available contrast agent DOTAREM (containing free Gd(DOTA) complex) was used for comparison. Relaxation times, T_1 and T_2, were measured at a concentration range of 0.12–1 mM of chelated Gd^{3+}. The relaxivities r_1 and r_2 were then calculated from the linear regression slope of $1/T_1$ and $1/T_2$ *vs.* Gd^{3+} concentration and are depicted in Figure 3. When Gd(DOTA) complex was attached to the dextran backbone of macromolecular Complex-2 or to the polysaccharide matrix of FUCO-Gd-SPs, both r_1 and r_2 relaxivities were enhanced with respect to DOTAREM. This effect was more pronounced in the case of FUCO-Gd-SPs with about twofold and fivefold increase in r_1 and r_2, respectively. As previously observed for other macromolecular or nanoparticulate contrast agents (Fransen et al., 2015; Huang et al., 2016; Courant et al., 2012), this relaxation rate enhancement can be ascribed to the restriction of the rotational motion of Gd(DOTA) complex inside polysaccharide matrix. In addition, the highly hydrated nature of FUCO-Gd-SPs network, would enhance Gd-water molecule interactions and favor the transfer of magnetic effect to the bulk water (Courant et al., 2012; De Sarno et al., 2019).

In order to check how the relaxometric properties translated in image contrast, the signal intensity of both T_1 and T_2-weighted images (Figure 4a-b) was as well quantified. While T_1-enhancing agents result in positive/brighter contrast, T_2 ones give predominantly negative/dark contrast. As shown in Figure 4c, positive contrast properties of FUCO-Gd-SPs were comparable to those of DOTAREM. However, FUCO-Gd-SPs appear to be a better

455 negative contrast agent in agreement with their significant higher r_2 relaxivity (Figure 4d).
456 Indeed, a signal void was present at high concentrations of Gd^{3+} (Figure 4b).

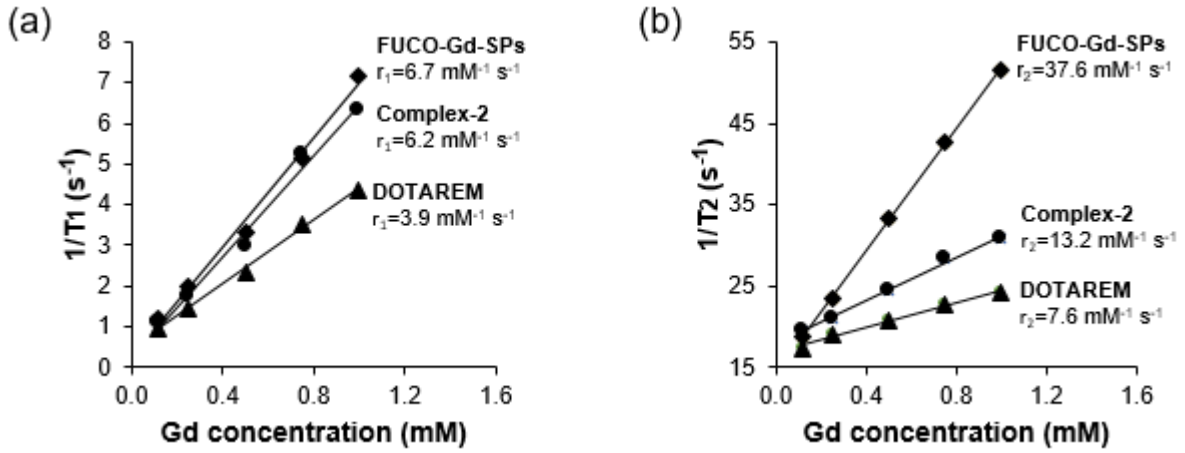

457

458 **Figure 3**. a) Longitudinal (r_1) and b) transversal (r_2) relaxation rates *vs*. Gd^{3+} concentration for
459 DOTAREM, Complex-2 and FUCO-Gd-SPs at 7 Tesla. The solid lines represent the linear regression
460 of the data. The slopes of the curves corresponding to relaxivity (r_1 or r_2) are indicated. Longitudinal
461 and transversal proton relaxivities of FUCO-Gd-SPs were 1.7 and 5.0 times higher than those of
462 DOTAREM.

463

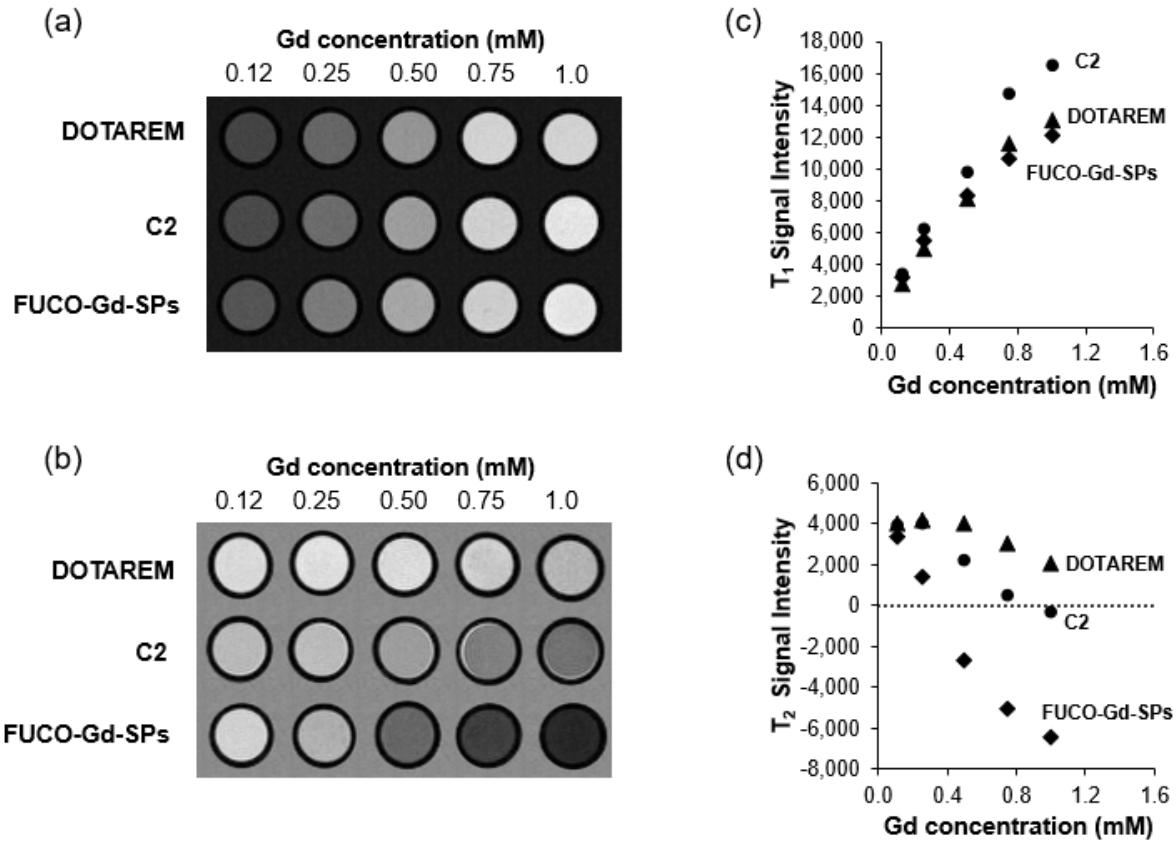

464

465 **Figure 4**. a) T_1 and b) T_2 weighted MRI acquisitions at 7 Tesla of DOTAREM, Complex-2 and
466 FUCO-Gd-SPs phantoms (agarose 2% (w/v)) used for relaxivity calculations. Background
467 corresponds to control (agarose gel with no Gd). Relative c) T_1 and d) T_2 weighted signal intensities
468 *versus* Gd concentration. FUCO-Gd-SPs showed enhanced negative contrast effect compared to
469 DOTAREM.

470

471 *3.5 Targeting properties*

472 The binding capacity of Gd-SPs and FUCO-Gd-SPs for P-selectin expressed onto the surface
473 of human activated platelets was assessed by flow cytometry in three conditions: platelet-rich
474 plasma (PRP), PRP with TRAP-activated platelets, and PRP with TRAP-activated platelets
475 after blocking P-selectin with a specific antibody (anti-CD62P). As shown on Figure 5a,
476 FITC-labeled FUCO-Gd-SPs strongly bound to activated platelets in absence of the antibody,

in agreement with the expression level of P-selectin in each condition (Figure S5). These results proved both the availability of some fucoidan chains at the surface of the polysaccharide matrix for interacting with P-selectin on activated platelets and the specificity of the interaction between fucoidan-functionalized SPs and P-selectin.

The binding of Gd-SPs and FUCO-Gd-SPs to platelet aggregates under arterial blood flow conditions was evaluated as well (Figure 5b). Experiments were performed in a flow chamber mimicking arterial blood flow conditions (wall shear stress of 67.5 dyn/cm^2) on activated platelet aggregates. FUCO-Gd-SPs (TRITC labeled) significantly accumulated at the surface of the aggregates whereas Gd-SPs showed almost no binding. Moreover, FUCO-Gd-SPs remained attached even after washing with 0.9% NaCl at arterial shear rate. These results confirmed the targeting ability of fucoidan-functionalized SPs under dynamic physiological conditions.

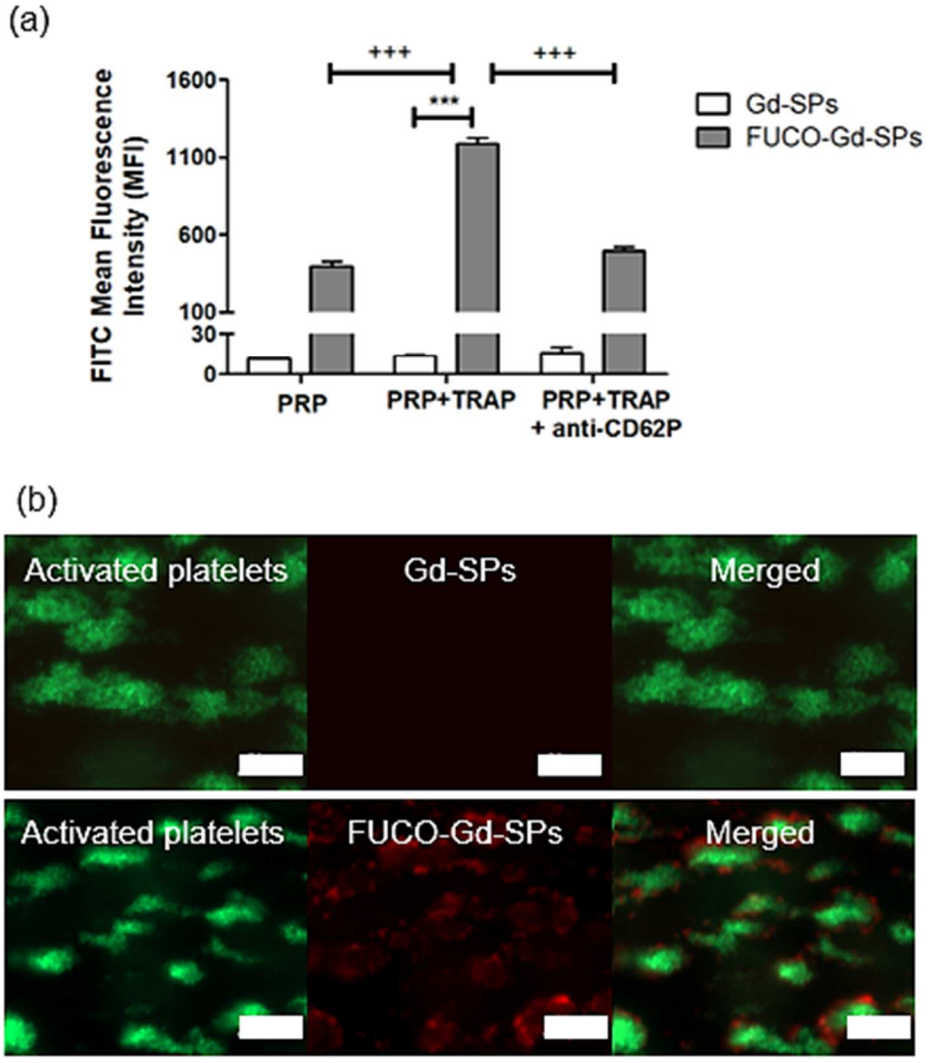

491

492 **Figure 5**. a) Flow cytometry assessment of interactions of FITC-labeled Gd-SPs and FITC-labeled
493 FUCO-Gd-SPs with either non-activated platelet-rich plasma (PRP), PRP activated with TRAP
494 (PRP+TRAP) and PRP activated with TRAP and blocked with P-selectin antibody (PRP+TRAP+anti-
495 CD62P) (Li et al., 2017). The mean fluorescence intensity (MFI) on the FITC channel was measured
496 for 10,000 events of PE-Cy5 labeled platelets at a particles concentration of 10 mg/mL (n=3;
497 ***p<0.001). b) Evaluation of FUCO-Gd-SPs binding on activated platelets under arterial flow
498 conditions (Li et al., 2017; Juenet et al., 2018). Human whole blood labeled with DiOC6 (green) was
499 injected into a collagen-coated microchannel to get platelets aggregates expressing P-selectin (left
500 images). TRITC-labeled particles (red) were then injected during 5 minutes (middle images). Channels
501 were washed with 0.9% NaCl after each step. Particles and platelets aggregates co-localization was

evaluated by merged fluorescence microscopy (right images). Gd-SPs (without fucoidan) were used as control. White scale bar corresponds to 50 µm.

4. Discussion

The driven idea of the approach presented here was to prepare a new diagnostic platform with the potential for Health agencies approval and human use. That's why we used non-harmful, biocompatible and biodegradable materials as both final particle constituents and preparation process raw materials. STMP was for instance preferred over conventional glutaraldehyde, a crosslinker with documented cytotoxicity (Oryan et al., 2018; Reddy et al., 2015). Biocompatible vegetable oil was, for its part, chosen as emulsion continuous phase instead of commonly used organic solvents. This choice supposed a challenge for the obtention of smaller particles as a highly viscous polysaccharide aqueous phase needed to be dispersed in a viscous oily phase. Reducing the size of our previous micrometric polysaccharide particles (Bonnard et al., 2014) to submicronic range, required the optimization of several processing parameters including vegetable oil and surfactant type, polysaccharide molecular weight and concentration, and so on. We obtained a final size of about 800 nm far above 100 nm widely admitted as a limit to efficiently avoid a rapid clearance from the reticuloendothelial system (RES). In previous studies we have evidenced *in vivo* interaction of fucoidan-bearing microparticule of 2.5 µm with aneurysmal thrombi (Bonnard et al., 2014; Li et al., 2017). Another key-parameter to limit the risk of quick RES uptake is the nature of the surface (De Jong & Borm, 2008). A polysaccharide coating may provide steric protection against protein adsorption (more particularly opsonins) and early macrophage uptake (Lemarchand et al., 2004). Anyway, the biological responses and biodistribution of our submicronic particles

remained to be investigated *in vivo*. Additional process optimization could further reduce, if needed, particle size.

Encapsulation of Gd-based contrast agents into polysaccharide nanoparticles have already been approached in three ways: by conjugation with polysaccharide precursor (Huang et al., 2008; Kim et al., 2015; Na et al., 2016; Nam et al., 2010; Payne et al., 2017; Zhang et al., 2015) , by ionic trapping during particles preparation (Gheran et al., 2018; Huang et al., 2008; Podgórna et al., 2017; Rigaux et al., 2017), or by post-modification of particles surface (Chan et al., 2015)**.** Nevertheless, Huang et al. demonstrated that Gd^{3+} ionically trapped into chitosan/dextran sulfate polyelectrolytes (PECs) is rapidly released after one day of incubation in PBS buffer at 37°C. In contrast, no release was detectable from Gd(DTPA)-grafted PECs under the same conditions during at least 6 days. Besides limiting the potential toxicity of free Gd ions, grafting of Gd-chelates to polysaccharide offers also the possibility to adjust Gd-cargo during particles synthesis. Herein, we gave the priority to the well-known and already clinically approved Gd(DOTA) complex. Gd(DOTA) was conjugated to an aminated dextran via a carbodiimide reaction and the resultant macrocomplexes were employed to synthesize both Gd-SPs and FUCO-Gd-SPs via the optimized emulsion-crosslinking method**.** By doing so, Gd(DOTA) groups were successfully incorporated to the designed platform conferring it dual positive and enhanced negative contrast properties (r_1= 6.7 mM^{-1} s^{-1} and r_2= 37.6 mM^{-1} s^{-1} at 7 T). Similar relaxation rates (r_1= 5.4 mM^{-1} s^{-1} and r_2= 36.4 mM^{-1} s^{-1}) were observed under the same magnetic field for self-assembled chitosan nanogels post-modified with Gd(DOTA) moieties (Chan et al., 2015). Increasing Gd cargo per particle would be particularly interesting to eventually improve T_1 relaxometric properties and decrease necessary doses for patients. This would probably require the optimization of the current dextran modification protocol or the implementation of another chemistry route leading to chemical bonds less sensitive to crosslinking in basic media. It is worth noting that our

imaging strategy is not only based on the contrast properties of the resulting SPs but also on their biospecificity. Low molecular weight fucoidan employed here as targeting agent recently passed preclinical evaluation as radiotracer for *in vivo* detection of cardiovascular pathologies (Chauvierre et al., 2019), and early stages of Phase I and Phase II clinical trials for its safety and validation of its ability to detect acute thrombosis in patients with suspected acute deep vein thrombosis are ongoing. Preferential accumulation of fucoidan-functionalized SPs onto thrombosed areas can be expected because of their binding affinity to activated platelets. This should rise the local concentration of contrast agent and increase thrombus imaging sensitivity of the FUCO-Gd-SPs compared to the commercial and non-biospecific DOTAREM at the same Gd dose.

5. Conclusions

Early detection of atherothrombotic lesions remains a big medical challenge. In this work, we developed novel biospecific polysaccharide submicronic particles containing Gd-based MR contrast agent. First, Gd(DOTA) moieties were successfully conjugated to dextran. The resulting macrocomplexes were then used to prepared Gd-loaded and fucoidan-functionalized particles by an emulsion-crosslinking method. This method was solvent-free in both production and purification steps. Particles exhibited good colloidal stability and were cytocompatible with human endothelial cells. The affinity of fucoidan-bearing particles for human activated platelets was evidenced under static and dynamic conditions. The particles exhibited good MR contrast properties with a significant signal enhancement of T_2-weighted images when compared to DOTAREM. These results indicated their high potential as a diagnostic probe for molecular imaging of atherothrombosis by MRI. As a next step, the

biospecificity of the particles and their capacity to image atherothrombosis will be checked *in-vivo* in experimental models of the disease.

Acknowledgments

The authors express their highest gratitude to Murielle Maire (LVTS, Villetaneuse, France) for fucoidan content determination, to Alina Zenych (LVTS, Paris, France) for some preliminary experiments, to Christine Choqueux (LVTS, Paris, France) and UTC (Compiègne, France) for SEM images, to Samira Benadda and CRI U1149 imaging facilities for confocal imaging training and to Stéphane Loyau and Kevin Guedj (LVTS, Paris, France) for flow cytometry experiment design and data analysis. We also thanks Rémi Le Borgne from the ImagoSeine facility (Jacques Monod Institute Paris, France), and the France BioImaging infrastructure supported by the French National Research Agency (ANR-10-INSB-04, « Investments fit the future ») for their precious help with TEM images.

This work was supported by INSERM, Université de Paris, Université Paris 13 and UMS34 FRIM, and received the financial support of the ANR-16-CE18-0031 NANOPACT**.**

REFERENCES

Abed, A., Assoul, N., Ba, M., Derkaoui, S. M., Portes, P., Louedec, L., Flaud, P., Bataille, I., Letourneur, D., & Meddahi-Pellé, A. (2011). Influence of polysaccharide composition on the biocompatibility of pullulan/dextran-based hydrogels. *Journal of Biomedical Materials Research Part A*, *96A*(3), 535–542. https://doi.org/10.1002/jbm.a.33007

Abir, F., Barkhordarian, S., & Sumpio, B. E. (2004). Efficacy of Dextran Solutions in Vascular Surgery. *Vascular and Endovascular Surgery*, *38*(6), 483–491. https://doi.org/10.1177/153857440403800601

596 Amirbekian, V., Lipinski, M. J., Briley-Saebo, K. C., Amirbekian, S., Aguinaldo, J. G. S.,
597 Weinreb, D. B., Vucic, E., Frias, J. C., Hyafil, F., Mani, V., Fisher, E. A., & Fayad, Z.
598 A. (2007). Detecting and assessing macrophages in vivo to evaluate atherosclerosis
599 noninvasively using molecular MRI. *Proceedings of the National Academy of*
600 *Sciences*, *104*(3), 961–966. https://doi.org/10.1073/pnas.0606281104
601 Antoniou, E., & Tsianou, M. (2012). Solution properties of dextran in water and in
602 formamide. *Journal of Applied Polymer Science*, *125*(3), 1681–1692.
603 https://doi.org/10.1002/app.35475
604 Bachelet, L., Bertholon, I., Lavigne, D., Vassy, R., Jandrot-Perrus, M., Chaubet, F., &
605 Letourneur, D. (2009). Affinity of low molecular weight fucoidan for P-selectin
606 triggers its binding to activated human platelets. *Biochimica et Biophysica Acta (BBA)*
607 *- General Subjects*, *1790*(2), 141–146. https://doi.org/10.1016/j.bbagen.2008.10.008
608 Barkhausen, J., Ebert, W., Heyer, C., Debatin, J. F., & Weinmann, H.-J. (2003). Detection of
609 Atherosclerotic Plaque With Gadofluorine-Enhanced Magnetic Resonance Imaging.
610 *Circulation*, *108*(5), 605–609. https://doi.org/10.1161/01.CIR.0000079099.36306.10
611 Bonnard, T., Serfaty, J.-M., Journé, C., Ho Tin Noe, B., Arnaud, D., Louedec, L., Derkaoui,
612 S. M., Letourneur, D., Chauvierre, C., & Le Visage, C. (2014). Leukocyte mimetic
613 polysaccharide microparticles tracked in vivo on activated endothelium and in
614 abdominal aortic aneurysm. *Acta Biomaterialia*, *10*(8), 3535–3545.
615 https://doi.org/10.1016/j.actbio.2014.04.015
616 Briley-Saebo, K. C., Shaw, P. X., Mulder, W. J. M., Choi, S.-H., Vucic, E., Aguinaldo, J. G.
617 S., Witztum, J. L., Fuster, V., Tsimikas, S., & Fayad, Z. A. (2008). Targeted
618 Molecular Probes for Imaging Atherosclerotic Lesions With Magnetic Resonance
619 Using Antibodies That Recognize Oxidation-Specific Epitopes. *Circulation*, *117*(25),
620 3206–3215. https://doi.org/10.1161/CIRCULATIONAHA.107.757120

621 Cai, K., Caruthers, S. D., Huang, W., Williams, T. A., Zhang, H., Wickline, S. A., Lanza, G.
622 M., & Winter, P. M. (2010). MR Molecular Imaging of Aortic Angiogenesis. *JACC:*
623 *Cardiovascular Imaging*, *3*(8), 824–832. https://doi.org/10.1016/j.jcmg.2010.03.012
624 Chan, M., Lux, J., Nishimura, T., Akiyoshi, K., & Almutairi, A. (2015). Long-Lasting and
625 Efficient Tumor Imaging Using a High Relaxivity Polysaccharide Nanogel Magnetic
626 Resonance Imaging Contrast Agent. *Biomacromolecules*, *16*(9), 2964–2971.
627 https://doi.org/10.1021/acs.biomac.5b00867
628 Caravan, P., Ellison, J. J., McMurry, T. J., & Lauffer, R. B. (1999). Gadolinium(III) Chelates
629 as MRI Contrast Agents: Structure, Dynamics, and Applications. *Chemical Reviews*,
630 *99*(9), 2293–2352. https://doi.org/10.1021/cr980440x
631 Chauvierre, C., Aid-Launais, R., Aerts, J., Chaubet, F., Maire, M., Chollet, L., Rolland, L.,
632 Bonafé, R., Rossi, S., Bussi, S., Cabella, C., Dézsi, L., Fülöp, T., Szebeni, J., Chahid,
633 Y., Zheng, K. H., Stroes, E. S. G., Le Guludec, D., Rouzet, F., & Letourneur, D.
634 (2019). Pharmaceutical Development and Safety Evaluation of a GMP-Grade
635 Fucoidan for Molecular Diagnosis of Cardiovascular Diseases. *Marine Drugs*, *17*(12),
636 699. https://doi.org/10.3390/md17120699
637 Chollet, L., Sabboural, P., Chauvierre, C., Villemin, J.-N., Letourneur, D., & Chaubet, F.
638 (2016). Fucoidans in Nanomedicine. *Marine Drugs*, *14*(8), 145.
639 https://doi.org/10.3390/md14080145
640 Corti, R., & Fuster, V. (2011). Imaging of atherosclerosis: magnetic resonance imaging.
641 *European Heart Journal*, *32*(14), 1709–1719. https://doi.org/10.1093/eurheartj/ehr068
642 Courant, T., Roullin, V. G., Cadiou, C., Callewaert, M., Andry, M. C., Portefaix, C., Hoeffel,
643 C., de Goltstein, M. C., Port, M., Laurent, S., Elst, L. V., Muller, R., Molinari, M., &
644 Chuburu, F. (2012). Hydrogels Incorporating GdDOTA: Towards Highly Efficient

Dual T1/T2 MRI Contrast Agents. *Angewandte Chemie International Edition*, *51*(36), 9119–9122. https://doi.org/10.1002/anie.201203190

De Jong, W. H., & Borm, P. J. A. (2008). Drug delivery and nanoparticles: Applications and hazards. *International Journal of Nanomedicine*, 133. https://doi.org/10.2147/IJN.S596

De Nooy, A. E. J., Rori, V., Masci, G., Dentini, M., & Crescenzi, V. (2000). Synthesis and preliminary characterisation of charged derivatives and hydrogels from scleroglucan. *Carbohydrate Research*, *324*(2), 116–126. https://doi.org/10.1016/S0008-6215(99)00286-4

De Sarno, F., Ponsiglione, A. M., Grimaldi, A. M., Netti, P. A., & Torino, E. (2019). Effect of crosslinking agent to design nanostructured hyaluronic acid-based hydrogels with improved relaxometric properties. *Carbohydrate Polymers*, *222*, 114991. https://doi.org/10.1016/j.carbpol.2019.114991

Dulong, V., Forbice, R., Condamine, E., Le Cerf, D., & Picton, L. (2011). Pullulan–STMP hydrogels: a way to correlate crosslinking mechanism, structure and physicochemical properties. *Polymer Bulletin*, *67*(3), 455–466. https://doi.org/10.1007/s00289-010-0435-2

Feng, X., Xia, Q., Yuan, L., Yang, X., & Wang, K. (2010). Impaired mitochondrial function and oxidative stress in rat cortical neurons: Implications for gadolinium-induced neurotoxicity. *NeuroToxicology*, *31*(4), 391–398. https://doi.org/10.1016/j.neuro.2010.04.003

Fransen, P., Pulido, D., Simón-Gracia, L., Candiota, A. P., Arús, C., Albericio, F., & Royo, M. (2015). r 1 and r 2 Relaxivities of Dendrons Based on a OEG-DTPA Architecture: Effect of Gd^{3+} Placement and Dendron Functionalization. *Journal of Nanotechnology*, *2015*, 1–8. https://doi.org/10.1155/2015/848020

Gheran, C., Rigaux, G., Callewaert, M., Berquand, A., Molinari, M., Chuburu, F., Voicu, S., & Dinischiotu, A. (2018). Biocompatibility of Gd-Loaded Chitosan-Hyaluronic Acid Nanogels as Contrast Agents for Magnetic Resonance Cancer Imaging. *Nanomaterials*, *8*(4), 201. https://doi.org/10.3390/nano8040201

Herrington, W., Lacey, B., Sherliker, P., Armitage, J., & Lewington, S. (2016). Epidemiology of Atherosclerosis and the Potential to Reduce the Global Burden of Atherothrombotic Disease. *Circulation Research*, *118*(4), 535–546. https://doi.org/10.1161/CIRCRESAHA.115.307611

Huang, M., Huang, Z. L., Bilgen, M., & Berkland, C. (2008). Magnetic resonance imaging of contrast-enhanced polyelectrolyte complexes. *Nanomedicine: Nanotechnology, Biology and Medicine*, *4*(1), 30–40. https://doi.org/10.1016/j.nano.2007.10.085

Huang, Y., Cao, J., Zhang, Q., Lu, Z., Hua, M., Zhang, X., & Gao, H. (2016). Chitosan oligosaccharide based Gd-DTPA complex as a potential bimodal magnetic resonance imaging contrast agent. *Magnetic Resonance Imaging*, *34*(1), 1–7. https://doi.org/10.1016/j.mri.2015.10.006

Jacques, V., Dumas, S., Sun, W.-C., Troughton, J. S., Greenfield, M. T., & Caravan, P. (2010). High-Relaxivity Magnetic Resonance Imaging Contrast Agents Part 2: Optimization of Inner- and Second-Sphere Relaxivity. *Investigative Radiology*, *45*(10), 613–624. https://doi.org/10.1097/RLI.0b013e3181ee6a49

Juenet, M., Aid-Launais, R., Li, B., Berger, A., Aerts, J., Ollivier, V., Nicoletti, A., Letourneur, D., & Chauvierre, C. (2018). Thrombolytic therapy based on fucoidan-functionalized polymer nanoparticles targeting P-selectin. *Biomaterials*, *156*, 204–216. https://doi.org/10.1016/j.biomaterials.2017.11.047

693 Kim, K. S., Park, W., & Na, K. (2015). Gadolinium-chelate nanoparticle entrapped human
694 mesenchymal stem cell via photochemical internalization for cancer diagnosis.
695 *Biomaterials*, *36*, 90–97. https://doi.org/10.1016/j.biomaterials.2014.09.014
696 Kuo, P. H., Kanal, E., Abu-Alfa, A. K., & Cowper, S. E. (2007). Gadolinium-based MR
697 Contrast Agents and Nephrogenic Systemic Fibrosis. *Radiology*, *242*(3), 647–649.
698 https://doi.org/10.1148/radiol.2423061640
699 Lack, S., Dulong, V., Picton, L., Cerf, D. L., & Condamine, E. (2007). High-resolution
700 nuclear magnetic resonance spectroscopy studies of polysaccharides crosslinked by
701 sodium trimetaphosphate: a proposal for the reaction mechanism. *Carbohydrate*
702 *Research*, *342*(7), 943–953. https://doi.org/10.1016/j.carres.2007.01.011
703 Leiner, T., Gerretsen, S., Botnar, R., Lutgens, E., Cappendijk, V., Kooi, E., & van
704 Engelshoven, J. (2005). Magnetic resonance imaging of atherosclerosis. *European*
705 *Radiology*, *15*(6), 1087–1099. https://doi.org/10.1007/s00330-005-2646-8
706 Lemarchand, C., Gref, R., & Couvreur, P. (2004). Polysaccharide-decorated nanoparticles.
707 *European Journal of Pharmaceutics and Biopharmaceutics*, *58*(2), 327–341.
708 https://doi.org/10.1016/j.ejpb.2004.02.016
709 Li, B., Juenet, M., Aid-Launais, R., Maire, M., Ollivier, V., Letourneur, D., & Chauvierre, C.
710 (2017). Development of Polymer Microcapsules Functionalized with Fucoidan to
711 Target P-Selectin Overexpressed in Cardiovascular Diseases. *Advanced Healthcare*
712 *Materials*, *6*(4), 1601200. https://doi.org/10.1002/adhm.201601200
713 Li, D., Patel, A. R., Klibanov, A. L., Kramer, C. M., Ruiz, M., Kang, B.-Y., Mehta, J. L.,
714 Beller, G. A., Glover, D. K., & Meyer, C. H. (2010). Molecular Imaging of
715 Atherosclerotic Plaques Targeted to Oxidized LDL Receptor LOX-1 by SPECT/CT
716 and Magnetic Resonance. *Circulation: Cardiovascular Imaging*, *3*(4), 464–472.
717 https://doi.org/10.1161/CIRCIMAGING.109.896654

718 Lino Ferreira, J. M. (2014), *Dextran-based materials for biomedical applications, 31-53*. M.
719 H. Gil.
720 Liu, H., Yuan, L., Yang, X., & Wang, K. (2003). La^{3+}, Gd^{3+} and Yb^{3+} induced changes in
721 mitochondrial structure, membrane permeability, cytochrome c release and
722 intracellular ROS level. *Chemico-Biological Interactions*, *146*(1), 27–37.
723 https://doi.org/10.1016/S0009-2797(03)00072-3
724 Lozano, R., Naghavi, M., Foreman, K., Lim, S., Shibuya, K., Aboyans, V., Abraham, J.,
725 Adair, T., Aggarwal, R., Ahn, S. Y., AlMazroa, M. A., Alvarado, M., Anderson, H.
726 R., Anderson, L. M., Andrews, K. G., Atkinson, C., Baddour, L. M., Barker-Collo, S.,
727 Bartels, D. H., … Murray, C. J. (2012). Global and regional mortality from 235 causes
728 of death for 20 age groups in 1990 and 2010: a systematic analysis for the Global
729 Burden of Disease Study 2010. *The Lancet*, *380*(9859), 2095–2128.
730 https://doi.org/10.1016/S0140-6736(12)61728-0
731 McAteer, M. A., Akhtar, A. M., von zur Muhlen, C., & Choudhury, R. P. (2010). An
732 approach to molecular imaging of atherosclerosis, thrombosis, and vascular
733 inflammation using microparticles of iron oxide. *Atherosclerosis*, *209*(1), 18–27.
734 https://doi.org/10.1016/j.atherosclerosis.2009.10.009
735 McEver, R. P. (2001). Adhesive interactions of leukocytes, platelets, and the vessel wall
736 during hemostasis and inflammation. *Thrombosis and Haemostasis*, *86*(3), 746–756.
737 Na, J. H., Lee, S., Koo, H., Han, H., Lee, K. E., Han, S. J., Choi, S. H., Kim, H., Lee, S.,
738 Kwon, I. C., Choi, K., & Kim, K. (2016). T_1-Weighted MR imaging of liver tumor by
739 gadolinium-encapsulated glycol chitosan nanoparticles without non-specific toxicity in
740 normal tissues. *Nanoscale*, *8*(18), 9736–9745. https://doi.org/10.1039/C5NR06673E
741 Naessens, M., Cerdobbel, A., Soetaert, W., & Vandamme, E. J. (2005). Leuconostoc
742 dextransucrase and dextran: production, properties and applications. *Journal of*

743 *Chemical Technology & Biotechnology*, *80*(8), 845–860.
744 https://doi.org/10.1002/jctb.1322
745 Nam, T., Park, S., Lee, S.-Y., Park, K., Choi, K., Song, I. C., Han, M. H., Leary, J. J., Yuk, S.
746 A., Kwon, I. C., Kim, K., & Jeong, S. Y. (2010). Tumor Targeting Chitosan
747 Nanoparticles for Dual-Modality Optical/MR Cancer Imaging. *Bioconjugate*
748 *Chemistry*, *21*(4), 578–582. https://doi.org/10.1021/bc900408z
749
750 Nguyen, T. N., Tinet, E., Ettori, D., Beilvert, A., Pavon-Djavid, G., Maire, M., Ou, P., Tualle,
751 J.-M., & Chaubet, F. (2017). Gadolinium/terbium hybrid macromolecular complexes
752 for bimodal imaging of atherothrombosis. *Journal of Biomedical Optics*, *22*(7), 76004.
753 https://doi.org/10.1117/1.JBO.22.7.076004
754 Nikolovski, B. G., Ilić, J. D., & Sovilj, M. N. (2016). HOW TO FORMULATE A STABLE
755 AND MONODISPERSE WATER-IN-OIL NANOEMULSION CONTAINING
756 PUMPKIN SEED OIL: THE USE OF MULTIOBJECTIVE OPTIMIZATION.
757 *Brazilian Journal of Chemical Engineering*, *33*(4), 919–931.
758 https://doi.org/10.1590/0104-6632.20160334s20140140
759 Oryan, A., Kamali, A., Moshiri, A., Baharvand, H., & Daemi, H. (2018). Chemical
760 crosslinking of biopolymeric scaffolds: Current knowledge and future directions of
761 crosslinked engineered bone scaffolds. *International Journal of Biological*
762 *Macromolecules*, *107*, 678–688. https://doi.org/10.1016/j.ijbiomac.2017.08.184
763 Payne, W. M., Hill, T. K., Svechkarev, D., Holmes, M. B., Sajja, B. R., & Mohs, A. M.
764 (2017). Multimodal Imaging Nanoparticles Derived from Hyaluronic Acid for
765 Integrated Preoperative and Intraoperative Cancer Imaging. *Contrast Media &*
766 *Molecular Imaging*, *2017*, 1–14. https://doi.org/10.1155/2017/9616791
767 Podgórna, K., Szczepanowicz, K., Piotrowski, M., Gajdošová, M., Štěpánek, F., &
768 Warszyński, P. (2017). Gadolinium alginate nanogels for theranostic applications.

Colloids and Surfaces B: Biointerfaces, *153*, 183–189. https://doi.org/10.1016/j.colsurfb.2017.02.026

Raggi, P., Baldassarre, D., Day, S., de Groot, E., & Fayad, Z. A. (2016). Non-invasive imaging of atherosclerosis regression with magnetic resonance to guide drug development. *Atherosclerosis*, *251*, 476–482. https://doi.org/10.1016/j.atherosclerosis.2016.06.028

Reddy, N., Reddy, R., & Jiang, Q. (2015). Crosslinking biopolymers for biomedical applications. *Trends in Biotechnology*, *33*(6), 362–369. https://doi.org/10.1016/j.tibtech.2015.03.008

Rigaux, G., Gheran, C. V., Callewaert, M., Cadiou, C., Voicu, S. N., Dinischiotu, A., Andry, M. C., Vander Elst, L., Laurent, S., Muller, R. N., Berquand, A., Molinari, M., Huclier-Markai, S., & Chuburu, F. (2017). Characterization of Gd loaded chitosan-TPP nanohydrogels by a multi-technique approach combining dynamic light scattering (DLS), asymetrical flow-field-flow-fractionation (AF4) and atomic force microscopy (AFM) and design of positive contrast agents for molecular resonance imaging (MRI). *Nanotechnology*, *28*(5), 055705. https://doi.org/10.1088/1361-6528/aa5188

Rogosnitzky, M., & Branch, S. (2016). Gadolinium-based contrast agent toxicity: a review of known and proposed mechanisms. *BioMetals*, *29*(3), 365–376. https://doi.org/10.1007/s10534-016-9931-7

Sabboural, P., Chaubet, F., Rouzet, F., Al-Shoukr, F., Azzouna, R., Bouchemal, N., Picton, L., Louedec, L., Maire, M., Rolland, L., Potier, G., Guludec, D., Letourneur, D., & Chauvierre, C. (2014). Purification of a Low Molecular Weight Fucoidan for SPECT Molecular Imaging of Myocardial Infarction. *Marine Drugs*, *12*(9), 4851–4867. https://doi.org/10.3390/md12094851

793 Sannino, A., Brevetti, L., Giugliano, G., Scudiero, F., Toscano, E., Mainolfi, C., Cuocolo, A.,
794 Perrino, C., Stabile, E., Trimarco, B., & Esposito, G. (2014). Non-invasive vulnerable
795 plaque imaging: how do we know that treatment works? *European Heart Journal -*
796 *Cardiovascular Imaging*, *15*(11), 1194–1202. https://doi.org/10.1093/ehjci/jeu097
797 Schroeder, A. P., & Falk, E. (1995). Vulnerable and dangerous coronary plaques.
798 *Atherosclerosis*, *118*, S141–S149. https://doi.org/10.1016/0021-9150(95)90081-0
799 Suzuki, M., Bachelet-Violette, L., Rouzet, F., Beilvert, A., Autret, G., Maire, M., Menager,
800 C., Louedec, L., Choqueux, C., Sabourał, P., Haddad, O., Chauvierre, C., Chaubet, F.,
801 Michel, J.-B., Serfaty, J.-M., & Letourneur, D. (2015). Ultrasmall superparamagnetic
802 iron oxide nanoparticles coated with fucoidan for molecular MRI of intraluminal
803 thrombus. *Nanomedicine*, *10*(1), 73–87. https://doi.org/10.2217/nnm.14.51
804 te Boekhorst, B. C., van Tilborg, G. A., Strijkers, G. J., & Nicolay, K. (2012). Molecular MRI
805 of Inflammation in Atherosclerosis. *Current Cardiovascular Imaging Reports*, *5*(1),
806 60–68. https://doi.org/10.1007/s12410-011-9114-4
807 van Tilborg, G. A. F., Vucic, E., Strijkers, G. J., Cormode, D. P., Mani, V., Skajaa, T.,
808 Reutelingsperger, C. P. M., Fayad, Z. A., Mulder, W. J. M., & Nicolay, K. (2010).
809 Annexin A5-Functionalized Bimodal Nanoparticles for MRI and Fluorescence
810 Imaging of Atherosclerotic Plaques. *Bioconjugate Chemistry*, *21*(10), 1794–1803.
811 https://doi.org/10.1021/bc100091q
812 Vananroye, A., Van Puyvelde, P., & Moldenaers, P. (2006). Effect of Confinement on
813 Droplet Breakup in Sheared Emulsions. *Langmuir*, *22*, 3972–3974.
814 https://doi.org/10.1021/la060442+
815 Waxman, S., Ishibashi, F., & Muller, J. E. (2006). Detection and Treatment of Vulnerable
816 Plaques and Vulnerable Patients: Novel Approaches to Prevention of Coronary

Events. *Circulation*, *114*(22), 2390–2411. https://doi.org/10.1161/CIRCULATIONAHA.105.540013

Yon, M., Billotey, C., & Marty, J.-D. (2019). Gadolinium-based contrast agents: From gadolinium complexes to colloidal systems. *International Journal of Pharmaceutics*, *569*, 118577. https://doi.org/10.1016/j.ijpharm.2019.118577

Zhang, L., Liu, T., Xiao, Y., Yu, D., & Zhang, N. (2015). Hyaluronic Acid-Chitosan Nanoparticles to Deliver Gd-DTPA for MR Cancer Imaging. *Nanomaterials*, *5*(3), 1379–1396. https://doi.org/10.3390/nano5031379

Zhao, J., Zhou, Z.-Q., Jin, J.-C., Yuan, L., He, H., Jiang, F.-L., Yang, X.-G., Dai, J., & Liu, Y. (2014). Mitochondrial dysfunction induced by different concentrations of gadolinium ion. *Chemosphere*, *100*, 194–199. https://doi.org/10.1016/j.chemosphere.2013.11.031

Zhou, Z., & Lu, Z.-R. (2013). Gadolinium-based contrast agents for magnetic resonance cancer imaging: Gadolinium-based CA for MR cancer imaging. *Wiley Interdisciplinary Reviews: Nanomedicine and Nanobiotechnology*, *5*(1), 1–18. https://doi.org/10.1002/wnan.1198

845 **GRAPHICAL ABSTRACT**

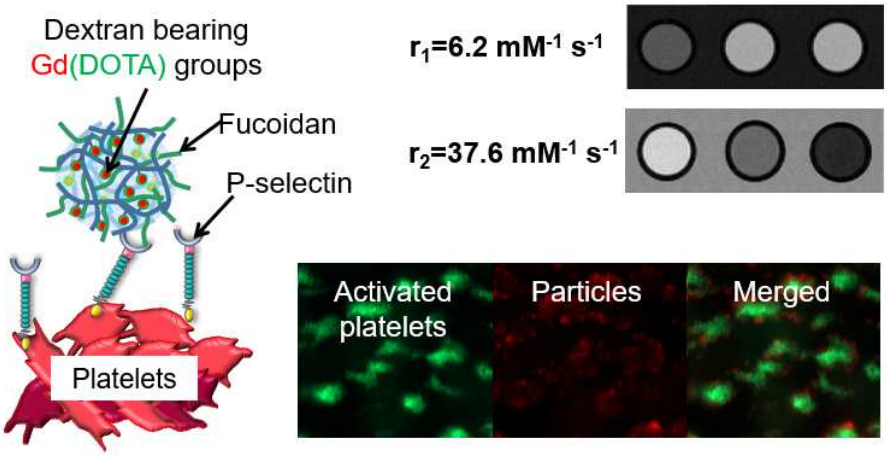

846

847